Distributed neural system for general intelligence revealed by lesion mapping

J. Gläscher[a,b,1], D. Rudrauf[c,d], R. Colom[e], L. K. Paul[a], D. Tranel[c], H. Damasio[f], and R. Adolphs[a,g]

[a]Division of Humanities and Social Sciences, California Institute of Technology, Pasadena, CA 91125; [b]Neuroimage Nord, Department of Systems Neuroscience, University Medical Center Hamburg-Eppendorf, 20246 Hamburg, Germany; [c]Department of Neurology and [d]Laboratory of Brain Imaging and Cognitive Neuroscience, University of Iowa, Iowa City, IA 52242; [e]Universidad Autonoma de Madrid, 28049 Madrid, Spain; [f]Dornsife Cognitive Neuroscience Imaging Center and Brain and Creativity Institute, University of Southern California, Los Angeles, CA 90089; and [g]Division of Biology, California Institute of Technology, Pasadena, CA 91125

Edited by Edward E. Smith, Columbia University, New York, NY, and approved January 25, 2010 (received for review September 10, 2009)

General intelligence (*g*) captures the performance variance shared across cognitive tasks and correlates with real-world success. Yet it remains debated whether *g* reflects the combined performance of brain systems involved in these tasks or draws on specialized systems mediating their interactions. Here we investigated the neural substrates of *g* in 241 patients with focal brain damage using voxel-based lesion–symptom mapping. A hierarchical factor analysis across multiple cognitive tasks was used to derive a robust measure of *g*. Statistically significant associations were found between *g* and damage to a remarkably circumscribed albeit distributed network in frontal and parietal cortex, critically including white matter association tracts and frontopolar cortex. We suggest that general intelligence draws on connections between regions that integrate verbal, visuospatial, working memory, and executive processes.

lesion patients | voxel-based lesion–symptom mapping | Wechsler Adult Intelligence Scale | white matter

Individual performances across a wide range of cognitive tasks are correlated: those people who perform well on some tasks tend to perform well across most tasks; those people who perform poorly on some tasks tend to perform poorly across most tasks. This effect is captured by the construct of general intelligence (or *g*), conceptualized by Spearman in 1904 (1) as that psychometric aspect of cognition whose variance is shared maximally across a wide variety of more specialized tests tapping verbal skills, spatial reasoning, memory, and other cognitive domains. There is strong evidence that Spearman's *g* is not merely a statistical abstraction but a distinct and pervasive cognitive ability. It comes into play in particular during demanding, effortful, nonautomated cognitive tasks requiring working memory capacity (2, 3). It is highly heritable (estimates are approximately 0.8) (4, 5), and it is a common source of inter-individual differences in all cognitive tasks (6). Furthermore, *g* is the psychological trait with the largest number of social and real-life correlates (e.g., income level and other measures of success) (7). Not surprisingly, efforts to understand its neurobiological substrate have been high on the list of priorities in fields ranging from biology to psychology and sociology. Here we address the question of whether *g* draws upon *specific* brain regions, as opposed to being correlated with global brain properties (such as total brain volume). Identifying such brain regions would help shed light on how *g* contributes to information processing and open the door to further exploration of its biological underpinnings, such as its emergence through evolution and development, and its alteration through psychiatric or neurological disease.

In the past 20 years a number of functional (3, 8, 9) and structural imaging studies (10–13), predominantly in healthy individuals and sometimes in combination with studies of heritability (5, 14), have investigated the neural signatures of *g*. Its neurobiological substrates have been variably linked to prefrontal cortex and the role of this brain region in cognitive control and flexibility (8), or instead to more distributed cortical regions (15). The latter account argues that *g* should involve interregional communication among many brain regions and therefore critically rely on the white matter connections between them, whereas the former account argues for a distinct region or network of regions implementing *g*. It thus remains debated whether *g* should be thought of as a single ability upon which other cognitive processes might draw, or whether it itself is constituted by the multiple cognitive processes from which it is psychometrically derived.

Here we investigated the neural substrates for *g* using nonparametric (16) voxel-based lesion–symptom mapping (VLSM) (17) in a large sample of 241 lesion patients (see Table S1 for demographic data) who had been tested on the Wechsler Adult Intelligence Scale (WAIS) (18) (see Table S2 for sample sizes and mean standardized scores on all WAIS subtests). VLSM compares, for every voxel, scores from patients with a lesion at that voxel contrasted against those without a lesion at that voxel. Unlike functional neuroimaging studies, which typically rely on the metabolic demands of gray matter and provide a purely correlational association between brain regions and cognitive processes (19), lesion mapping methods can identify regions, including white matter tracts, playing a causal role in a particular cognitive domain by mapping where damage can interfere with performance (20). We used hierarchical factor analysis across multiple cognitive tasks (10, 21) to derive a robust measure of *g* and found statistically significant associations between *g* and damage to a remarkably circumscribed albeit distributed set of regions in left frontal and right parietal cortex, as well as white matter association tracts connecting these sectors. These findings suggest that *g* reflects the ability to effectively integrate verbal, visuospatial, working memory, and executive processes via a circumscribed set of cortical connections.

Results

Extracting *g* with Hierarchical Factor Analysis. Spearman's *g* is often measured using problem-solving tasks like Raven's Advanced Progressive Matrices (RAPM) (3, 9, 22) that require relational integration across different stimulus dimensions (23). However, using a single task runs counter to the cross-task variance concept of *g* (1). A procedure more in keeping with the original psychometric construct involves extracting *g* from a battery of cognitive tests using hierarchical factor analysis (Schmid-Leiman transformation, SLT) (10, 21), in which the loadings of the primary variables on a second-order *g* factor take precedence over the loadings on the first-order factors. Using this approach (see

Author contributions: J.G. and R.A. designed research; D.T. and H.D. performed research; H.D. contributed new reagents/analytic tools; J.G., D.R., and R.C. analyzed data; and J.G., D.R., R.C., L.K.P., D.T., H.D., and R.A. wrote the paper.

The authors declare no conflict of interest.

This article is a PNAS Direct Submission.

Freely available online through the PNAS open access option.

[1]To whom correspondence should be addressed. E-mail: glascher@hss.caltech.edu.

This article contains supporting information online at www.pnas.org/cgi/content/full/0910397107/DCSupplemental.

Materials and Methods for details), we extracted *g* and three first-order factors (verbal abilities, visuospatial abilities, and working memory) from nine WAIS subtests chosen for their unequivocal expression of a well-known factor structure (Fig. 1). The SLT revealed that all verbal subtests (loadings: 0.57–0.66) as well as the Arithmetic (0.67) and Block Design (0.57) subtests exhibit high loadings on *g*, consistent with previous accounts (10). A direct comparison of the first-order loading matrix before and after SLT (Fig. 1 *A* and *B*) further showed that the factor structure is clearly preserved in our lesion patients, even after accounting for *g*. This confirmed that *g* absorbed the shared variance among the subtests without perturbing the psychometric architecture of the three domain-specific factors, yielding an accurate measure of *g* that abstracts from any specific cognitive ability.

To confirm the robustness of our measure of *g*, we conducted two additional analyses. First, we extracted *g* using the same hierarchical factor analysis as above, but only from a reduced sample of 117 subjects, who had complete data sets on all WAIS subtests. This analysis yielded very similar *g* and first-order loading matrices (Fig. S1), which was confirmed by a highly significant similarity coefficient (R_V = 0.92, Z = 14.24, P < 0.0001) (24). Second, to demonstrate the robustness of *g* across different tasks, we replicated this *g* extraction using different sets of WAIS subsets (Table S3, Table S4, and Table S5).In all cases the *g* scores were very similar (correlations ranged from 0.97 to 0.99), underlining the robustness of our approach.

Lesion Mapping of *g*. Our main VLSM analysis related all participants' *g* factor scores to the lesion pattern in the sample. Statistical power maps (Fig. S2) confirmed that we had sufficient power in most regions to detect a significant relationship between lesion location and *g* with a 5% false discovery rate (FDR) threshold in the VLSM analysis (16). Significant effects were prominently located in the left hemisphere and encompassed expected locations of major white matter fiber tracts, including the anterior and dorsal bundle of the superior longitudinal/arcuate fasciculus connecting temporal, parietal, and inferior frontal regions, the superior frontooccipital fasciculus connecting dorsolateral prefrontal cortex (DLPFC) and possibly the frontal pole with the superior parietal lobule (25), and the uncinate fasciculus, which connects anterior temporal cortex and amygdala with orbitofrontal and frontal polar regions. Right hemispheric loci were found in the occipitoparietal junction reaching into the postcentral sulcus and in the anterior bank of the central sulcus (Fig. 2). These findings lend support to a connectivity account of *g*: *g* critically draws on efficient communication between multiple brain regions, which is instantiated by major association tracts connecting brain regions in the inferior frontal and superior parietal lobe (15).

To further test the hypothesis that a neural substrate of *g* might involve the integration among regions that implement more specific cognitive abilities, we next examined the overlap between the location of voxels significantly associated with *g* and with each of the individual WAIS subtests. We reasoned that the anatomic conjunction of individual subtest effects with the *g*-related effect could help elucidate the extent to which *g* is implemented in the aggregate of all cognitive processes working together, or whether *g* is constituted by a more abstract overarching subset or superset as implied by its psychometric derivation. Fig. 1*C* shows the percentage of overlapping voxels associated with *g* and with each subtest for each hemisphere separately. The index was computed as the number of overlapping voxels normalized by the number of voxels within the union of *g* and each subtest [overlap/(*g* ∪ subtest], which takes into account that there may be unique voxels associated with *g* or with any of the subtests.

This analysis revealed only a modest overlap for Picture Arrangement (0.10), Block Design (0.09), and Picture Completion (0.08), indicating that visuospatial skills are vulnerable to damage in much larger areas of the right hemisphere than those involved in *g* (Fig. S3). However, working memory and verbal skills overlapped more substantially with the left hemispheric correlate of *g*, most notably for the Arithmetic (0.42) and Similarities (0.39) subtests. These particular subtests rely heavily on the capacity for complex reasoning and integration of various forms of knowledge and cognitive processes, in addition to basic verbal and working memory skills. As such, they recruit skills from a distributed area of cortex and depend on cortical connections (26). Likewise, Similarities requires integration of various forms of knowledge and cognitive processes to generate abstract conceptualizations (26). Thus it seems that the neural substrate of *g* involves long-range connections that are broadly distributed throughout the cortex and yet a more circumscribed neural substrate than that of the underlying select skills (Fig. S3).

Is there a neural region whose damage uniquely impacts *g* but not any of the nine WAIS subtests from which *g* is psychometrically derived? We addressed this question by examining the nonoverlap between a disjunction (logical "OR") of all WAIS

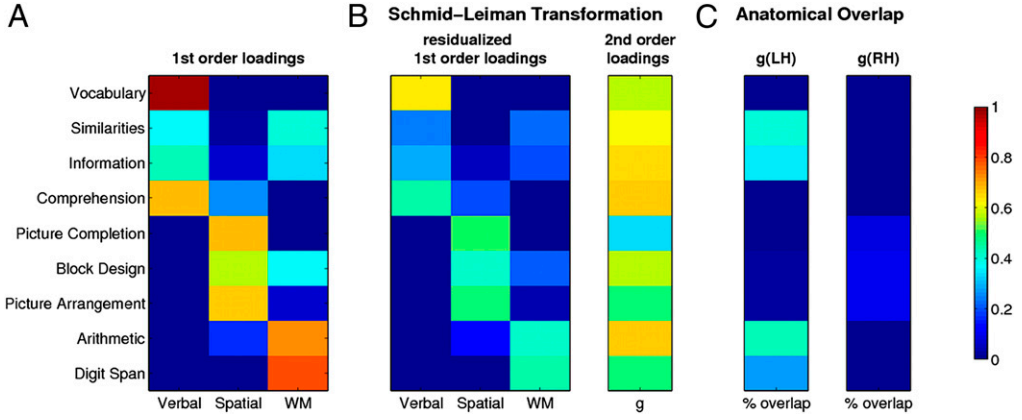

Fig. 1. Extracting Spearman's *g* using hierarchical factor analysis. (*A*) Loading matrix for nine WAIS subtests onto three first-order factors [denoted "verbal," "spatial," and "working memory" (WM)] extracted from a promax-rotated common factor analysis using principal axis factoring. (*B*) Loading matrices after applying the Schmid-Leiman transformation (see *Materials and Methods* for details). The second-order factor (*g*) absorbs as much variance in the primary variables (subtests) as possible, and the first-order factors are reduced to partial correlations. (*C*) Voxelwise percentage of anatomical overlap between *g* and WAIS subtests computed as the number of voxels in the overlap divided by the number of voxels in the union of *g* and each subtest. For clarity, the significant anatomic regions for *g* (Fig. 2) were separated into left and right hemispheres. A more detailed view of the overlap can be found in Fig. S3.

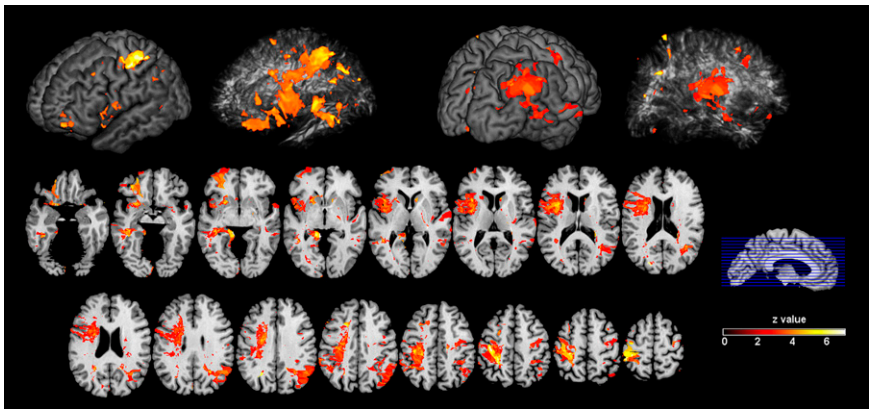

Fig. 2. Lesion mapping of *g*. 3D renderings show cortical and subcortical regions with a statistically significant relationship between lesion location and *g* (corrected at 5% FDR). Axial slices are shown for a more detailed inspection.

subtests and the lesion pattern found for *g* (Fig. 3). This analysis revealed a single region in the left frontal pole [Brodmann Area (BA) 10] that showed a significant effect unique to *g*.

Discussion

In this study we investigated the specific neural correlates of general intelligence (*g*), a psychological construct predicated on the fact that test performances on most cognitive tasks are positively correlated. Using hierarchical factor analysis (SLT), we measured *g* in a sample of 241 patients with stable chronic brain lesions and used VLSM (16, 17) to identify brain structures associated with *g*. We found a significant effect on *g* with lesions in left hemispheric white matter sectors including the arcuate and superior longitudinal fasciculus that connect the frontal and parietal lobe. In addition, we found a sector in the left anterior frontal pole (BA 10) that is uniquely related to *g* and not shared with any other cognitive test.

It is striking that, despite its distributed nature, the neural substrate of *g* reported here is remarkably circumscribed, concentrated in the core of white matter, and essentially always comprises a narrow subset of the regions associated with performance on individual WAIS subtests. The largest overlap between WAIS subtests and *g* was found for Arithmetic, Similarities, Information, and Digit Span; the former two tests also exhibited the greatest conjunction with *g*. These subtests assess verbal knowledge about the world, verbal reasoning, and abstraction, as well as working memory capacity, and are associated with the left inferior frontal gyrus, the superior longitudinal/arcuate fascicule, and to some degree with parietal cortex (27) (Fig. S3). This suggests that *g* draws on the combination of conceptual know ledge and working memory, and that the communication between areas associated with these capacities is of crucial importance (2). Such an interpretation is consistent with the Parieto-Frontal Integration Theory (P-FIT) (15), which postulates roles for cortical regions in the prefrontal (BA 6, 9–10, 45–47), parietal (BA 7, 39–40), occipital (BA 18–19), and temporal association cortex (BA 21, 37). Our results emphasize the important role of white matter tracts in binding the proposed regions together into a unified system subserving *g*, in line with a recent study relating white matter integrity to intellectual performance (28): the study reported significant correlations between integrity of the superior fronto-occipital fasciculus and full-scale intelligence quotient (IQ) (a measure related, but not identical, to *g*).

Working memory, which seems to be left lateralized when tested in the verbal domain (29), is considered a key cognitive ability strongly related to *g* (2, 3, 30). The white matter tracts identified in our analysis connect ventrolateral prefrontal cortex (VLPFC) and DLPFC with the inferior parietal cortex and terminate in the superior parietal lobule. In general, VLPFC is associated with processing intentions and switches between cognitive sets, which—in the context of working memory—could correspond to stimulus–response mappings underlying successful performance (31). By contrast, the DLPFC is thought to be involved in the manipulation of items in working memory (31). Finally, the left posterior parietal cortex has been associated with the storage of verbal material in working memory (32).

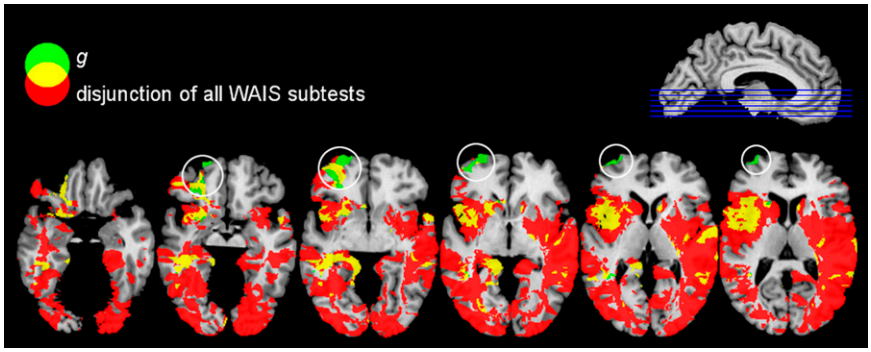

Fig. 3. Overlap (yellow) of *g* (green) and a disjunction (logical "OR") of nine WAIS subtests (red) thresholded at 5% FDR. A region in the left frontal pole (white circles) is unique to *g* and not captured by any other subtest. Immediately adjacent (left lateral orbitofrontal cortex and underlying white matter) lies the significant lesion–deficit effect for the Information subtest from the WAIS, which partially overlaps with the unique frontal polar region for *g* (two leftmost circles).

Although our findings generally support the P-FIT model, they also suggest that a sector of prefrontal cortex may play a unique role in *g* (Fig. 3). Interestingly, this region (left lateral aspect of BA 10) has been also associated with increased blood oxygen level–dependent (BOLD) activity during a variety of higher-order cognitive processes (23), including retrieval of abstract semantic knowledge, as is required for the Similarities subtest (33), as well as difficult problem-solving tasks akin to the RAPM (34), a test commonly used to measure *g* (3, 9, 15, 22). Our finding of a unique neural correlate of *g* in BA 10 argues for another, distinct aspect complementing the distributed processing discussed above: the need for hierarchical processing control. BA 10 has a documented role in cognitive control and subgoal processing (35–38) and may thus be involved in the allocation of the working memory resources necessary for successful performance on specific cognitive tasks. Taken together, our findings argue that *g* may critically rely on efficient interregional communication subserving processes for configuring and holding items in working memory, along with a hierarchical component for flexible control in the frontopolar cortex. Such an interpretation would be consistent, respectively, with the fluid information processing nature of *g* as well as its effortful "executive" aspect (8, 30).

It could be argued that the high *g* loadings of the verbal scales are driving the predominant left lateralization that we observed. However, if *g* was dominated by purely verbal performance (as captured in the "verbal" factor in our factor analysis; Fig. 1*A*), then *g* should have picked up more shared variance from these scales, leading to a disproportionate reduction of first-order "verbal" loadings after the SLT (Fig. 1*B*). This was, however, not generally the case. The largest attenuations of first-order loadings were found for Vocabulary, Arithmetic, and Digit Span (Fig. S4), the latter two originally belonging to the working memory factor, which reinforces our suggestion that working memory and the frontoparietal regions it involves contributes largely to *g* (2, 3, 26, 27).

An interesting question pertains to the stability of *g* as a psychological trait across the lifespan. The age de-differentiation hypothesis predicts an increasing contribution of *g* to cognitive performances during the later stages of life (39). This would predict that *g* explains a greater amount of task variance in older subjects. We tested this hypothesis in our sample by dividing the subject sample into young and old subjects (median-split) but found no support for the hypothesis (percentage explained variance: young subjects, 36.0%; old subjects, 30.6%). This lack of support for the age de-differentiation hypothesis is consistent with earlier work (40, 41).

In conclusion, we show that *g* draws on a distributed but circumscribed set of cortical regions and their white matter connections. These comprise regions related to working memory capacity, verbal and visuospatial processing, subserved by a frontoparietal system, along with an executive component subserved by left frontopolar cortex. Two closing caveats should be noted. First, given that lesions influencing *g* were found in both hemispheres, we would expect commissural tracts to contribute significantly. However, these were underrepresented in our lesion sample and thus may not have been detected. Second, Spearman's *g* disregards theories of multiple intelligences (42) and does not incorporate specific emotional abilities (43). Therefore we may have isolated an anatomical network important for processing external stimuli, which might operate in parallel with others that are more critical for stimulus reward processing and interoception.

Materials and Methods

Subjects and Neuropsychological Data. The WAIS-R and/or WAIS-III was administered to 241 neurologic patients who were being evaluated in connection with their enrollment in the Iowa Cognitive Neuroscience Patient Registry at the University of Iowa, over the course of approximately 2 decades. When only WAIS-R data were available, the subtest scores were converted to WAIS-III equivalents according to the standardized scores reported in the WAIS-III manual. Under the auspices of the Registry, the patients had been extensively characterized in terms of their neuropsychologic (44) and neuroanatomic status (45). Demographic data are given in Table S1. Where multiple datasets were available, we chose neuropsychological and neuroanatomical datasets that were as contemporaneous as possible. All patients had single, focal, stable, chronic lesions of the brain, and the Registry excludes patients with progressive disease or psychiatric illness. All subjects had given written informed consent to participate in these research studies.

Neuroanatomical Data. All neuroanatomical data were mapped using MAP-3, as described previously (45, 46). Briefly, the visible lesion in each subject's MRI or CT scan was manually traced, slice by slice, onto corresponding regions of a single, normal reference brain (template brain) that has been used in all prior studies with this method. All of the lesions were traced by a single expert (H.D.) who has demonstrated high reliability (47). This manual tracing was only done when confidence could be achieved for matching corresponding slices between the lesion brain and the reference brain. Thus, lesions were only mapped, if (*i*) they were clearly distinguishable from the (possibly dilated) ventricular system, (*ii*) there were no coexisting signs of cortical atrophy, and (*iii*) the MRI or CT scan showed no imaging artifact. Because the neuroanatomical data were manually traced to a stereotaxic template, no automated spatial normalization was required. The lesion maps for each subject were resampled to an isotropic voxel size of 1 mm^3, spatially smoothed with a 4-mm full-width-at-half-maximum (FWHM) Gaussian kernel, binarized at a threshold of 0.2, and finally converted to the NiFTI file format.

Hierarchical Factor Analysis. We computed *g* loadings from 9 WAIS subtests and individual *g* factor scores using a two-stage Schmid-Leiman hierarchical factor analyis (48), which has been recommended as the preferential method for extracting a *g* factor (49). In the original data matrix **Z** of 241 patients missing data were replaced by the mean. We then analyzed the data correlation matrix **R** in a common factor analysis and extracted three promax-rotated principal factors, resulting in the first-order loading matrix **P1** shown in Fig. 1*A*. The factor correlation matrix **F** of this first-order factor analysis was analyzed in a second-order common factor analysis extracting a single factor (*g*) resulting in a second-order loading matrix **P2**.

In the framework of the Schmid-Leiman factor transformation, loadings for the primary variables (WAIS subtests) onto the second-order factor (*g*) take precedence over loadings onto the first-order factors (verbal, spatial, and working memory), which are reduced to part correlations (50) and thus differ from the loadings of the initial factor analyses above (Fig. 1*B*). The residualized first-order loading matrix is computed by postmultiplying the original first-order loading matrix **P1** with the second-order uniqueness **U2**: $\mathbf{P1SL = P \times U2}$ (Fig. 1*B*). Similarly, the *g* loadings of the primary variables (WAIS subtests) were determined by multiplication of both loading matrices: $\mathbf{P2SL = P1 \times P2}$ (Fig. 1*B*).

Following ref. 51, we computed factor scores using regression of the data correlation matrix **R** onto the first-order structure matrix $\mathbf{S = P1 \times F}$. Parameter estimates **B** were determined by $\mathbf{B = R^{-1} \times S}$. These parameter estimates were rescaled using a diagonal matrix $\mathbf{D = sqrt[diag(B^T \times S)]^{-1}}$. The resulting weighting matrix $\mathbf{W = B \times D}$ was used to project the original data onto the residualized first-order factor space: $\mathbf{FS = Z \times W}$, where **FS** are the factor scores. An analogous procedure was used to determine *g* factor scores.

Extraction *g* from the WAIS and Comparison of Different Factor Solutions. We selected nine WAIS subtests for extracting *g*. Three subtests (Matrix Reasoning, Letter–Number Sequencing, and Symbol Search) were undersampled ($n < 100$) compared with the rest of the subtests, because these are unique to the WAIS-III and therefore not administered to all of our patients. We therefore excluded these from our final set. Table S2 lists the means, SDs, and sample sizes of all WAIS subtests.

The WAIS exhibits a robust first-order factor structure, which is used to derive index scores for three factors: (*i*) *verbal* (Vocabulary, Similarities, Information, and Comprehension), (*ii*) *spatial* (Picture Completion, Block Design, and Picture Arrangement), and (*iii*) *working memory* (Digit Span and Arithmetic) (10). This factor structure was used to extract *g* loadings and factor scores. Here, however, to demonstrate the robustness of our extraction of *g* we report the factor solutions for 10 and 13 WAIS subtests for comparison with the solution for 9 subtests used as the main analysis (Table S3, Table S4, and Table S5). The *g* factor scores derived from either solution were highly correlated: r(WAIS13, WAIS9) = 0.97, r(WAIS13, WAIS10) = 0.98, r(WAIS10, WAIS9) = 0.99.

Lesion Analysis of *g* Factor Scores. The *g* factor scores were used for nonparametric (16) VLSM (17) as implemented in "Nonparametric Mapping," which is part of the MRIcron software package (http://www.sph.sc.edu/comd/rorden/

mricron/). This mass-univariate analysis compares the *g* factor scores between patients with and without a lesion at each and every voxel in the brain. It uses the Brunner-Munzel test, a nonparametric variant of the two-sample *t* test that allows for heteroscedasticity of the variances in both groups (52). We used a threshold of 5% FDR (53) to control for multiple comparisons and an extent threshold of 50 voxels per cluster. Maps of statistical power (54) were computed to verify that we had sufficient coverage to detect a significant lesion–deficit relationship in almost the entire brain (Fig. S2). These power calculations (16) use the nonparametric Wilcoxon-Mann-Whitney probability to estimate a power *threshold*. For instance, had our sample size been only 10 patients of whom (at a particular voxel) only 3 had a lesion, then the most extreme ranking would be W = 6 (sum of the rank 1, 2, and 3), which corresponds to a *P* value of 0.01667 or a *Z* value of 2.13. Therefore, if our statistical threshold corresponding to a 5% FDR threshold had been *Z* = 2.56, we would not expect to detect this voxel not matter how large the effect size actually is.

ACKNOWLEDGMENTS. We thank Prof. M. Spezio for fruitful discussions of methodological issues; and Prof. M. Cassell (University of Iowa) for neuranatomical advice regarding white matter tracts. This work was supported by Akademie der Naturforscher Leopoldina Grant 9901/8-140 (to J.G.) and by National Institutes of Health Grants P01NS19632 (to D.T., H.D., and R.A.), R01DA022549 (to D.T.), and R01MH080721 (to R.A.), a grant by the Simons Foundation to R.A., as well as by the Tamagawa University global Centers of Excellence Program of the Japanese Ministry of Education, Culture, Sports, and Technology. R.C. was funded by Grant SEJ-2006-07890 from the Ministry of Education and Culture, Spain, and Grant PR2008-0038 from the Ministry of Science and Innovation, Spain.

1. Spearman C (1904) General intelligence objectively determined and measured. *Am J Psychol* 15:201–293.
2. Conway AR, Kane MJ, Engle RW (2003) Working memory capacity and its relation to general intelligence. *Trends Cogn Sci* 7:547–552.
3. Gray JR, Chabris CF, Braver TS (2003) Neural mechanisms of general fluid intelligence. *Nat Neurosci* 6:316–322.
4. Plomin R, DeFries JC, Craig IW, McGuffin P (2003) *Behavioral Genetics in a Post-Genomic Era* (American Psychological Association, Washington, DC).
5. Posthuma D, et al. (2002) The association between brain volume and intelligence is of genetic origin. *Nat Neurosci* 5:83–84.
6. Johnson W, te Nijenhuis J, Bouchard TJ, Jr. (2008) Still just 1 *g*: Consistent results from five test batteries. *Intelligence* 36:81–95.
7. Gottfredson LS (1997) Why g matters: The complexity of everyday life. *Intelligence* 24: 79–132.
8. Duncan J, et al. (2000) A neural basis for general intelligence. *Science* 289:457–460.
9. Lee KH, et al. (2006) Neural correlates of superior intelligence: Stronger recruitment of posterior parietal cortex. *Neuroimage* 29:578–586.
10. Colom R, Jung RE, Haier RJ (2006) Distributed brain sites for the g-factor of intelligence. *Neuroimage* 31:1359–1365.
11. Haier RJ, Jung RE, Yeo RA, Head K, Alkire MT (2004) Structural brain variation and general intelligence. *Neuroimage* 23:425–433.
12. Shaw P, et al. (2006) Intellectual ability and cortical development in children and adolescents. *Nature* 440:676–679.
13. Narr KL, et al. (2007) Relationships between IQ and regional cortical gray matter thickness in healthy adults. *Cereb Cortex* 17:2163–2171.
14. Thompson PM, et al. (2001) Genetic influences on brain structure. *Nat Neurosci* 4: 1253–1258.
15. Jung RE, Haier RJ (2007) The Parieto-Frontal Integration Theory (P-FIT) of intelligence: Converging neuroimaging evidence. *Behav Brain Sci* 30:135–154, discussion 154–187.
16. Rorden C, Karnath HO, Bonilha L (2007) Improving lesion-symptom mapping. *J Cogn Neurosci* 19:1081–1088.
17. Bates E, et al. (2003) Voxel-based lesion-symptom mapping. *Nat Neurosci* 6:448–450.
18. Wechsler D (1997) *Wechsler Adult Intelligence Scale* (The Psychological Corporation, San Antonio, TX), 3rd Ed.
19. Price CJ, Mummery CJ, Moore CJ, Frakowiak RS, Friston KJ (1999) Delineating necessary and sufficient neural systems with functional imaging studies of neuropsychological patients. *J Cogn Neurosci* 11:371–382.
20. Rudrauf D, Mehta S, Grabowski TJ (2008) Disconnection's renaissance takes shape: Formal incorporation in group-level lesion studies. *Cortex* 44:1084–1096.
21. Haier RJ, et al. (2009) Gray matter and intelligence factors: Is there a neuro-*g*? *Intelligence* 37:136–144.
22. Colom R, et al. (2009) Gray matter correlates of fluid, crystallized, and spatial intelligence: Testing the P-FIT model. *Intelligence* 37:124–135.
23. Ramnani N, Owen AM (2004) Anterior prefrontal cortex: Insights into function from anatomy and neuroimaging. *Nat Rev Neurosci* 5:184–194.
24. Abdi H (2007) RV coefficient and congruence coefficient. *Encyclopedia of Measurement and Statistics*, ed Salkind N (Sage, Thousand Oaks, CA), pp 849–853.
25. Catani M, Howard RJ, Pajevic S, Jones DK (2002) Virtual in vivo interactive dissection of white matter fasciculi in the human brain. *Neuroimage* 17:77–94.
26. Lezak MD, Howieson DB, Loring DW (2004) *Neuropsychological Assessment* (Oxford Univ Press, Oxford), 4th Ed.
27. Gläscher J, et al. (2009) Lesion mapping of cognitive abilities linked to intelligence. *Neuron* 61:681–691.
28. Chiang MC, et al. (2009) Genetics of brain fiber architecture and intellectual performance. *J Neurosci* 29:2212–2224.
29. Wager TD, Smith EE (2003) Neuroimaging studies of working memory: A meta-analysis. *Cogn Affect Behav Neurosci* 3:255–274.
30. Duncan J (2005) Frontal lobe function and general intelligence: Why it matters. *Cortex* 41:215–217.
31. Owen AM, McMillan KM, Laird AR, Bullmore E (2005) N-back working memory paradigm: A meta-analysis of normative functional neuroimaging studies. *Hum Brain Mapp* 25:46–59.
32. Smith EE, Jonides J (1998) Neuroimaging analyses of human working memory. *Proc Natl Acad Sci USA* 95:12061–12068.
33. Goldberg RF, Perfetti CA, Fiez JA, Schneider W (2007) Selective retrieval of abstract semantic knowledge in left prefrontal cortex. *J Neurosci* 27:3790–3798.
34. Christoff K, et al. (2001) Rostrolateral prefrontal cortex involvement in relational integration during reasoning. *Neuroimage* 14:1136–1149.
35. Koechlin E, Basso G, Pietrini P, Panzer S, Grafman J (1999) The role of the anterior prefrontal cortex in human cognition. *Nature* 399:148–151.
36. Koechlin E, Hyafil A (2007) Anterior prefrontal function and the limits of human decision-making. *Science* 318:594–598.
37. Badre D, Wagner AD (2004) Selection, integration, and conflict monitoring; assessing the nature and generality of prefrontal cognitive control mechanisms. *Neuron* 41: 473–487.
38. Braver TS, Bongiolatti SR (2002) The role of frontopolar cortex in subgoal processing during working memory. *Neuroimage* 15:523–536.
39. Balinsky B (1941) An analysis of the mental factors of various age groups from nine to sixty. *Genet Psychol Monogr* 23:191–234.
40. Juan-Espinosa M, et al. (2002) Age dedifferentiation hypothesis: Evidence from the WAIS III. *Intelligence* 30:395–408.
41. Escorial S, Juan-Espinosa M, Garcia LF, Rebollo I, Colom R (2003) Does *g* change in adulthood? Testing the age de-differentiation hypothesis across sex. *Pers Individ Dif* 34:1525–1532.
42. Gardner H (1983) *Frames of Mind. The Theory of Multiple Intelligences* (Basic Books, New York).
43. Salovey P, Mayer JD (1990) Emotional intelligence. *Imagination Cogn Pers* 9:185–211.
44. Tranel D (2007) Theories of clinical neuropsychology and brain-behavior relationships: Luria and beyond. *Textbook of Clinical Neuropsychology*, eds Morgan JE, Ricker JH (Taylor and Francis, New York), pp 27–37.
45. Frank RJ, Damasio H, Grabowski TJ (1997) Brainvox: An interactive, multimodal visualization and analysis system for neuroanatomical imaging. *Neuroimage* 5:13–30.
46. Damasio H, Frank R (1992) Three-dimensional in vivo mapping of brain lesions in humans. *Arch Neurol* 49:137–143.
47. Fiez JA, Damasio H, Grabowski TJ (2000) Lesion segmentation and manual warping to a reference brain: Intra- and interobserver reliability. *Hum Brain Mapp* 9:192–211.
48. Schmid J, Leiman JM (1957) The development of hierarchical factor solutions. *Psychometrika* 22:83–90.
49. Jensen AR, Weng LJ (1994) What is a good g? *Intelligence* 18:231–258.
50. Wolff HG, Preising K (2005) Exploring item and higher order factor structure with the Schmid-Leiman solution: Syntax codes for SPSS and SAS. *Behav Res Methods* 37:48–58.
51. Loehlin JC (1998) *Latent Variable Models: An Introduction to Factor, Path and Structural Analysis* (Lawrence Erlbaum Associates, Mahwah, NJ), 3rd Ed.
52. Brunner E, Munzel U (2000) The nonparametric Behrens-Fisher problem: Asymptotic theory and a small-sample approximation. *Biometr J* 42:17–25.
53. Nichols T, Hayasaka S (2003) Controlling the familywise error rate in functional neuroimaging: A comparative review. *Stat Methods Med Res* 12:419–446.
54. Rudrauf D, et al. (2008) Thresholding lesion overlap difference maps: Application to category-related naming and recognition deficits. *Neuroimage* 41:970–984.